

Cite this: *Lab Chip*, 2015, 15, 3838

## Miniaturized optogenetic neural implants: a review

B. Fan and W. Li\*

Optogenetics is an exciting new technology that allows targetable fast control and readout of specific neural populations in complex brain circuits. With the rapid development of light-sensitive microbial opsins, substantial gains in understanding the causal relationships between neural activity and behavior in both healthy and diseased brains have been achieved during the last decade. However, the intricate and complex interactions between different neural populations in mammalian brains require novel, implantable, neural interfaces that are capable of manipulating and probing targeted neurons at multiple sites and with high spatiotemporal resolution. Advanced microtechnology has offered the highest potential to meet these demands of optogenetic applications. In this paper, we review a variety of miniaturized optogenetic neural implants developed in recent years, based on different light sources, including lasers, laser diodes, and light-emitting diodes. We then summarize the specifications of these microimplants and their related microfabrication approaches and discuss the major challenges of current techniques and the vision for the future of the field.

Received 27th May 2015,

Accepted 11th August 2015

DOI: 10.1039/c5lc00588d

[www.rsc.org/loc](http://www.rsc.org/loc)

### I. Introduction

The complex brain networks comprise billions of interconnected neurons with diverse types, shapes, sizes, and activity patterns. Targeted access to specific neural populations with high spatiotemporal resolution enables the study of neural circuits and cellular conditions for both fundamental understanding of brain functions and development of therapeutic strategies for many brain injuries and disorders. While well-established microelectrophysiological methods have been successfully used to record neural activity at single-cell resolution,<sup>1</sup> neuromodulation with electrical modality, which initiates neural functional response by injecting a biphasic current to depolarize the membranes of nerve cells,<sup>2</sup> suffers from indiscriminate stimulation of cell components (somas, dendrites, and axons) as well as poor spatial resolution due to unpredictable current pathways.<sup>3</sup>

Recent advances in optogenetics provide a unique neuromodulation technique, allowing optical control of genetically targeted specific neurons that express light-sensitive opsin proteins. Optical stimulation of neurons was first demonstrated in 1971,<sup>4</sup> when action potentials in *Aplysia* ganglia were excited using high-power blue laser light. In 2003, a new era for the optical stimulation of mammalian neurons started with the discovery of a light-sensitive ion

channel, Channelrhodopsin-2 (ChR2),<sup>5</sup> followed by the discovery of an optically activated chloride pump, Halorhodopsin (NpHR),<sup>6</sup> and a proton pump, Archaeorhodopsin (Arch).<sup>7</sup> Neurons that express these light-sensitive opsins can be depolarized (for neural excitation) or hyperpolarized (for neural inhibition) by visible light at appropriate wavelengths with millisecond temporal accuracy.<sup>8</sup> Multiple opsins can also be expressed in a single cell so that the same cell can be selectively excited or inhibited with the corresponding light.<sup>9,10</sup> The cell-type specificity of optogenetics is achieved by selecting appropriate promoters, for example, human synapsin I for targeting neurons, CamKIIα for targeting excitatory neurons, glial fibrillary acidic protein for targeting astroglia, and ppHcrt promoter for targeting hypocretin neurons in rodents.<sup>11,12</sup> Other practical advantages of optogenetics over electrical stimulation include minimal instrumental interferences with simultaneous electrophysiological recording as well as scalable optical tools to access large-scale neural networks. These merits of optogenetics have opened a new door for neuroscientists to study brain mapping,<sup>13,14</sup> retinal prosthesis,<sup>15</sup> physiology disorder,<sup>16</sup> Parkinson's disease, epilepsy,<sup>17</sup> and cardiac electrophysiology,<sup>18</sup> which cannot be achieved using conventional electrical stimulation modality.

Current progress toward the development of optogenetic tools has followed two parallel paths, one focusing on the development of light-gated microbial opsins for the genetic modification of normal neurons and the other on the development of optics and photonics for light delivery. To date, a wide variety of naturally occurring and synthetic microbial

Electrical and Computer Engineering Department, Michigan State University, East Lansing, MI 48824, USA. E-mail: fanbin@msu.edu, wenli@egr.msu.edu;  
Tel: +1 517 353 7832

opsins have been engineered to enable optical excitation, inhibition, bi-stable modulation, and control of electrical and biochemical signaling in neurons and other cell types, as published in.<sup>19–22</sup> Recent breakthroughs in highly sensitive ChR2 and NpHR genes have enabled optogenetic neuromodulation with low light intensity.<sup>22–24</sup> In order to fully realize the remarkable potential of these opsins, engineering tools for simultaneous light delivery and electrophysiological recording are needed. For *in vitro* light delivery, in 2005, Boyden *et al.*<sup>8</sup> demonstrated reliable, millisecond, single-component, genetically targeted optical neuromodulation, where ChR2-expressing hippocampal neurons were excited using an incandescent lamp (450–490 nm, 300 W) with a Chroma excitation filter, and the light-induced neural activity was recorded using a whole-cell patch clamp. Following that, Ishizuka *et al.*<sup>25</sup> utilized a surface-mounted, blue-light-emitting diode (LED) (470–490 nm) to quantify the relationship between the light-gated current and the intensity of blue light illumination on ChR2-expressing hippocampal cell cultures. Other *in vitro* optical instruments have also been reported, such as a focused laser beam using acousto-optic deflectors<sup>26</sup> and digital micro-mirror devices (DMDs).<sup>27,28</sup> Although these *in vitro* approaches can successfully activate neural activity in both cultured neuronal and acute slice preparation, they are not suitable for *in vivo* stimulation in the intact brain or for study in freely behaving animals.

The first demonstration of functional optical control of intact animal brains was reported in 2007 by Dr. Deisseroth's group at Stanford University.<sup>29</sup> In their studies, the motor cortex of living rodents was stimulated through an intracranial, multimode, optical fiber coupled to a solid-state laser diode system, with an output light intensity of ~380 mW mm<sup>-2</sup>. Since then, many implantable light-delivery systems have been implemented by coupling a thick optical fiber of a few hundred microns to a laser or LED light source. Such systems have been used to study the light-evoked neural activity as well as behavioral changes in commonly used animal models, both small (mice/rats)<sup>30–34</sup> and large (non-human primates).<sup>35–38</sup> These systems, however, inevitably activate many uninterested neurons and are impractical in the spatial control of multi-site stimulation in large-scale neural networks. Therefore, there has been an increased need for the development of implantable, reliable light delivery and recording interfaces with high spatiotemporal resolution and spectral control ability.<sup>20</sup>

Recently, advanced microfabrication techniques have been investigated to construct and miniaturize optical neural implants capable of multi-site, localized light stimulation of three-dimensional (3D) brain networks with fine spatial resolution. These devices can be categorized into two major groups based on different light sources: laser, including laser diodes and diode-pumped solid-state (DPSS) laser diodes, and LEDs, including bulk LEDs and microscale LEDs ( $\mu$ LEDs). Optical fibers, microwave guides, channel waveguides, and tapered optrodes are most commonly used to guide light from sources to target neurons. Microfabricated probes with  $\mu$ LEDs mounted directly at the tip of the probe

shaft have also been implemented by several groups. Furthermore, monolithic integration of miniaturized optical elements with multi-electrodes and wireless interfaces enables spatially confined optical stimulation and simultaneous recording of light-evoked neural activity in freely moving animals.

In this paper, we review some of the representative micro-implants for optogenetic applications and their related fabrication technologies. First, section I discusses the state-of-the-art technology of light delivery tools. Section II summarizes microscale optical implants based on lasers or laser diodes. Section III is devoted to microimplants based on LED light sources. Section IV introduces the recent development of wirelessly powered and controlled optical neural implants. Section V discusses several challenges for current optogenetic neural implants, especially for  $\mu$ LED-based microdevices. Such challenges include thermal management, photoelectric artifacts, material compatibility and safety, and complicated fabrication. Finally, section VI provides concluding remarks and a vision for the future development of implantable optogenetic neural interfaces.

## II. Laser-coupled optical neural implants

Effective photostimulation of optogenetic opsins requires a minimum irradiance of 1 (or 7) mW mm<sup>-2</sup> for neural excitation (or inhibition).<sup>39</sup> The practical requirement of irradiance is also affected by the high degree of light scattering and absorption in neural tissue.<sup>20</sup> For these reasons, fiber-coupled lasers with high power are being widely used as light sources for many optogenetic experiments.<sup>31,39–42</sup> A laser can generate coherent light with unique characteristics: low divergence to focus the light beam over a long distance and high temporal coherence to confine the bandwidth of emitted light within a narrow spectrum. The former characteristic allows light to be steered through optical fibers to target cells with lower loss than with incoherent light sources (e.g. LEDs). This results in more efficient coupling between light sources and fibers with thin core diameters of 50  $\mu$ m or less. The latter characteristic enables high efficiency of optical stimulation since the majority of irradiance will fall into the peak activation spectra of microbial opsins and contribute to optical stimulation. To deliver laser light into target cells, waveguiding structures must be used and are typically implemented by several fabrication techniques, including glass-sharpened optical fibers, out-of-plane microwaveguide arrays, and in-plane microwaveguide probes. In the following sections, we discuss the device configurations and fabrication techniques of different laser-coupled, optical neural interfaces. Representative prototypes are presented in Fig. 1, and their specifications are summarized in Table 1.

### 2.1. Glass-sharpened optical fibers

Single-site, laser-coupled optical fibers are typically made of commercially available multimode optical fibers with core

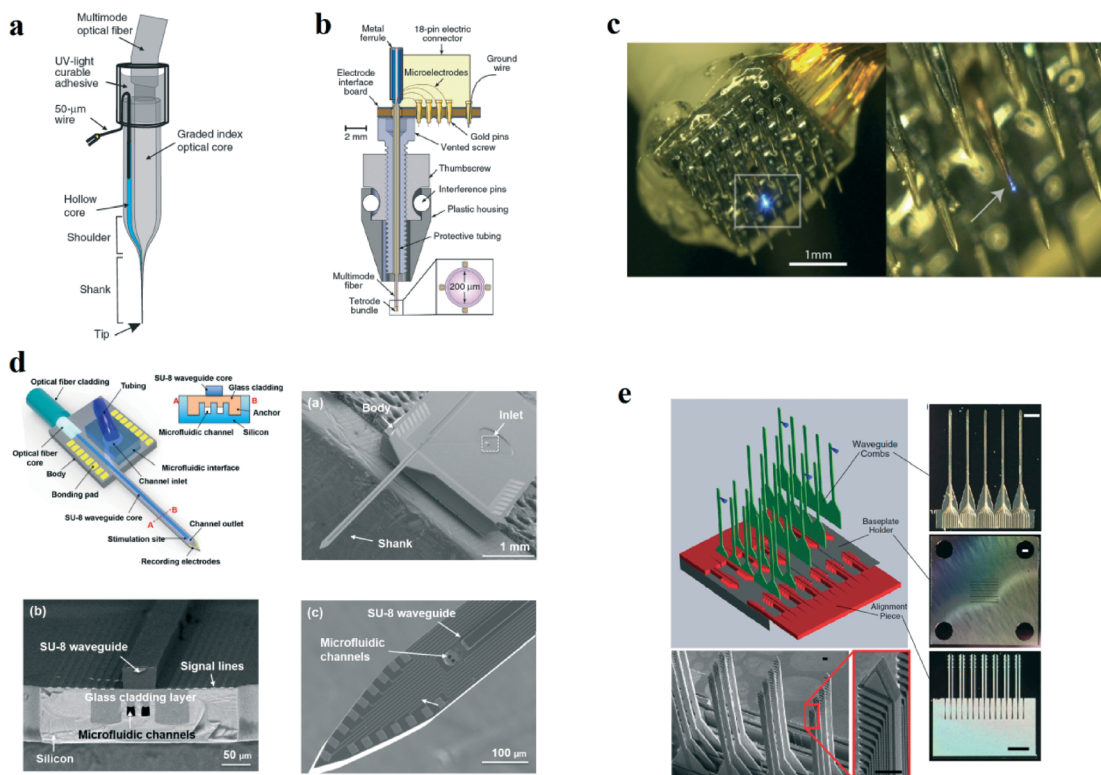


**Fig. 1** Examples of laser-based optical neural interfaces. (a) A dual-core optical fiber system with one optical core for optical stimulation and one hollow core filled up with 1–3 M NaCl for electrical recording. Reprinted from ref. 41. (b) A multimode optical fiber with four tetrode bundles attached for electrophysiological recording. Reprinted from ref. 31. (c) A dual-mode optrode array adapted from a Utah multielectrode array, where one recording shank was replaced with a multimode optical fiber. Reprinted from ref. 49. (d) An in-plane neural probe adapted from conventional Michigan neural probe with embedded dielectric waveguides and microfluidic channels. Reprinted from ref. 53. (e) A 3D multiwaveguide array consisting of a set of waveguide combs assembled on a base plate holder through two alignment and fixation pieces. Reprinted from ref. 59.

diameters of ~200 μm. To reduce the thickness of a multimode fiber for localized optical stimulation, in some approaches the plastic cladding layer of the fiber was stripped and the bare glass core with a minimum diameter of 100 μm was guided into a rodent brain through an implanted cannula.<sup>19,40</sup> Wet chemical etching is often employed to sharpen the tip of the glass core in order to further improve spatial resolution and minimize the tissue damage during device insertion. For example, Eran Stark *et al.*<sup>39</sup> reported a stepped optical fiber, which consisted of a 5 mm-long segment with a diameter of 60–70 μm and an overetched tip formed into a cone (~12°), fabricated by pulling the optical fiber at the hydrofluoric acid/mineral oil interface with various speeds and durations. The ability to use single-site, implanted optical fibers for simultaneous optical stimulation and neural recording has also been demonstrated by several groups. Recently, Polina Anikeeva *et al.*<sup>31</sup> (Fig. 1(a)) combined a multimode optical fiber attached with four tetrode bundles for electrophysiological recording. Additionally, a dual-core optical fiber system was developed by Yoan LeChasseur *et al.*<sup>41</sup> (Fig. 1(b)) and Suzie Dufour *et al.*,<sup>42</sup> with one optical core for optical stimulation and one hollow core filled with 1–3 M NaCl for electrical recording. The probe was pulled to a tip size smaller than a neuron soma. Optical stimulation was achieved by coupling the probe to a laser source

through a multimode optical fiber. Similarly, a dual-modal, tungsten microelectrode-based optrode that enclosed optical fibers within its insulation glass was constructed by binding optical fibers and a tungsten wire tightly to each other and then integrally coating the bundle with a smooth, thin layer of glass.<sup>43</sup>

Key advantages of these implantable microfibers include flexibility to adjust stimulation depth, fabrication/assembly simplicity, and low cost. However, limited by single-site stimulation, these devices cannot be applied to optical control across large-scale brain networks and different cortical layers,<sup>14</sup> which requires multi-site optical stimulation and recording capabilities. In addition, the separation between optical fiber and recording sites cannot be precisely controlled by manual alignment and assembly.

## 2.2. Out-of-plane microwave guide arrays

Recently, out-of-plane microwave guide arrays have been developed, allowing selective and dynamic optical stimulation of a single or multiple brain regions. These devices are normally micromachined, employing thin out-of-plane waveguide shanks with tapered tips to improve spatial resolution and reduce implant invasiveness. Light illuminated by laser light sources is butt-coupled to the waveguide shank and

**Table 1** Summary of the specification of miniaturized, laser-based optogenetic neural implants

Optical neurostimulation components				Electrical recording components						
Light source	# of channels	Dimensions	Output light intensity/energy (max. or used in test)	Light delivery efficiency	# of channels	Dimensions	1 kHz impedance	Other capabilities	Substrate material	Ref.
Optical fiber coupled waveguide (oxynitride core)	1	70 $\mu\text{m}$ wide	7 mW $\text{mm}^{-2}$	-10.5 ± 1.9 dB	8	143 $\mu\text{m}^2$ in diameter, 20 $\mu\text{m}$ separation	1.37 M $\Omega$	No	Si	50
Bare laser chip coupled waveguide (SU8 core)	1 × 2	15 $\mu\text{m}$ wide, 13 $\mu\text{m}$ long	29.7 mW $\text{mm}^{-2}$ @ 659 nm	—	2 × 4	20 $\mu\text{m}$ in diameter	1.54 ± 0.06 M $\Omega$	No	Si	51
Optical fiber coupled waveguide (SU8)	1	0.15 mm in width	60 mW $\text{mm}^{-2}$	-12 dB	8	—	280 K $\Omega$ -350 K $\Omega$	Micro-fluidic channel	Polyimide	52
Optical fiber coupled waveguide (SU8)	1	≤150 $\mu\text{m}$ wide	0.9 mW	—	16	~20 $\mu\text{m}$ × 20 $\mu\text{m}$	0.8 M $\Omega$	Micro-fluidic channel	Si	53
Optical fiber coupled multi-waveguide (oxynitride core)	12	60~360 $\mu\text{m}$ wide, 1 cm long, 1 mm separation	—	-10 dB	0	—	—	No	Quartz	55
Tapered optical fiber with multi-openings	Max. 7	600 nm in diameter	3.5 mW	—	0	—	—	No	—	60
Laser-3D waveguide	192	9 $\mu\text{m}$ × 60 $\mu\text{m}$	#1 scheme: 148 ± 56 mW $\text{mm}^{-2}$ , #2 scheme: 200 mW $\text{mm}^{-2}$	#1 scheme: 17.3 ± 1.8 dB, #2 scheme: 11.9 ± 2.5 dB	0	—	—	No	Si	59
Laser-coupled fiber	1	200 $\mu\text{m}$ in diameter	~380 mW $\text{mm}^{-2}$	—	0	—	—	No	—	29
Laser-coupled fiber	1	200 $\mu\text{m}$ in diameter	60–160 mW $\text{mm}^{-2}$ @ 473 nm, 160–260 mW $\text{mm}^{-2}$ @ 561 nm	—	4	Diameter ~25 $\mu\text{m}$	—	No	—	31
Laser-coupled fiber	1	Tip diameter of 6–20 $\mu\text{m}$ , fiber diameter of 4 $\mu\text{m}$	≤10 mW $\text{mm}^{-2}$	—	1	0.7 $\mu\text{m}$ in diameter	—	No	—	41
Laser-coupled optrode	1	50–62.5 $\mu\text{m}$ in diameter	916 mW $\text{mm}^{-2}$	-1.55 dB	99	1 mm long, 400 $\mu\text{m}$ separation	112–671 K $\Omega$	No	—	46
Laser-coupled optrode	100	0.5–2 mm long, 150 $\mu\text{m}$ wide 400 $\mu\text{m}$ separation	—	-1.49 dB	0	—	—	No	SiO <sub>2</sub>	45

then emitted from the tip for neural stimulation. The shank length and taper slope of the waveguide are carefully engineered to minimize the optical loss due to Fresnel and internal reflection. It was evident that power loss and output beam divergence are greater for shorter, more tapered waveguides.<sup>44</sup> The optical waveguides can be readily integrated with silicon Utah multielectrode probes for simultaneous stimulation and recording of neural activity.

One such device is an SiO<sub>2</sub> Utah waveguide array capable of optical stimulation with both visible and infrared (IR)

light. This device consists of 10 × 10 arrays of optrodes 0.5 mm to 2 mm long at a 400  $\mu\text{m}$  pitch, constructed by bulk micromachining fused silica or quartz dices of 3 mm thickness and 50 mm diameter. A dicing saw with a bevel blade was used to shape the pyramidal tips with a precisely controlled taper slope.<sup>45</sup> Furthermore, Jiayi Zhang *et al.* reported a dual-modal optrode array<sup>46–49</sup> (Fig. 1(c)) (Blackrock Microsystems) modified from a previously developed silicon Utah multielectrode array. In their design, one of the 100 silicon shanks was replaced with a multimode optical fiber by

removing a shank, drilling a hole using ablative laser machining, inserting the fiber mechanically through the hole, and then bonding the fiber with adhesive epoxy. Although these out-of-plane arrays provide an alternative solution to manipulating and mapping large brain regions with improved spatial resolution, device fabrication heavily relies on specialized bulk micromachining and dicing techniques, which are complicated and cannot be easily adopted by other researchers. In addition, the function of the 100-channel glass waveguide array for multi-site optogenetic stimulation has not yet been validated *in vitro* or *in vivo*.

### 2.3. In-plane microwave guide probe

Compared to the out-of-plane arrays, in-plane micro waveguide probes benefit more from modern microelectromechanical system (MEMS) technology evolved from process technology in conventional semiconductor device fabrication. Most of these probes share a similar configuration: an in-plane microwaveguide for light delivery carried by a silicon or polymer shaft with electrophysiological recording and/or microfluidic modalities. Several combinations of dielectric materials used for microwaveguides include an oxynitride core (refractive index: 1.51) with oxide clad (refractive index: 1.46)<sup>50</sup> and an SU-8 core with either silicon oxide,<sup>51</sup> tungsten-titanium alloy (10% titanium),<sup>52</sup> or glass clad.<sup>53</sup> The multilayer, core-shell structures of the microwaveguides are usually constructed based on planar micromachining technology. Alternating layers of dielectric thin films are deposited and patterned using ultraviolet (UV) photolithography and etching (wet or dry) techniques. Fabrication of the microelectrode probe shafts follows the process techniques well established for making conventional Michigan neural probes.<sup>54</sup> For the two designs with microfluidic modality, integrated microchannels are constructed by either photopatterning of SU-8 (ref. 52) or reflow of borosilicate glass followed by chemical mechanical polishing (CMP)<sup>53</sup> (Fig. 1(d)). Light coupling between laser light sources and planar microwaveguides is typically achieved through optical fibers. For efficient coupling, grooves<sup>50,53</sup> are made on the probe shafts using deep reactive ion etching (DRIE) or custom-designed optical adapters<sup>52</sup> in order to precisely align and secure optical fibers in a fixed position relative to the microwave guides. Alternatively, Michael Schwaerzel *et al.*<sup>51</sup> demonstrated the direct coupling of light from a bare laser diode chip to an SU-8 microwave guide without the use of optical fibers. Although this design enables an ultra compact size and the possibility of wireless powering, no *in vivo* validation was reported to demonstrate effective optogenetic neuromodulation through directly coupled light.

Despite their significant advantages, the aforementioned devices are limited to delivering light to a single target and therefore not suitable for applications that require delivering patterned light independently to distributed targets in 3D brain circuits, such as in the rhesus macaque cortex.<sup>55</sup> From a fabrication perspective, a straightforward approach to

increase the spatial density of optical stimulation is to assemble 3D arrays with planar, multi shank waveguide probes, using possible methods originally developed for 3D Michigan-type multielectrode arrays. Such methods include backbone stacking and bonding,<sup>56</sup> folded Parylene cable,<sup>57</sup> and orthogonal insertion of planar probes into a carrying platform.<sup>58</sup> Making planar waveguide probes with multiple shafts can be achieved simply by modifying photomask designs without increasing the complexity of device fabrication. However, the spatial density is still limited by the number of shafts. Therefore, the ability to deliver light through multiple sites along a single probe shaft will provide a major breakthrough for high-resolution spatial photostimulation.

Recently, optical probes with spatially distributed emitting sites along a single probe shaft were reported by Anthony N. Zorzos *et al.*<sup>55</sup> In this approach, 12 varying-length dielectric microwave guides were lithographically patterned on the same shaft, with smooth bends coated with aluminum as corner mirrors at the outputs of individual waveguides. As the waveguides can be separately coupled to different light sources, this device enables independently addressable optical stimulation at each output with adjustable wavelength and various light delivery efficiency of 23–33% depending on the length of the waveguide. To expand the spatial resolution into three dimensions, a 3D multiwaveguide array<sup>59</sup> (Fig. 1(e)) was implemented consisting of a set of waveguide combs inserted orthogonally into a base plate holder with the assistance of two alignment and fixation pieces. These devices, while successfully demonstrated, still have a large footprint due to the requirements of multiple waveguides and light sources. Most recently, Ferruccio Pisanello *et al.*<sup>60</sup> further improved the spatial resolution of multipoint-emitting optical probes by utilizing a focused ion beam (FIB) system to mill several emitting windows along a tapered optical fiber. Emitting site selection was achieved by adjusting the angle of incident light on the input of the fiber. The use of a single tapered fiber minimizes implant invasiveness. While this device presents significant advantages in terms of selective and dynamic illumination at different brain regions, the maximum out-coupling efficiency varies with the locations of the emitting windows due to mode evanescence. In addition, the power and the angle of incident light must be carefully tuned in order to maintain the extinction ratios of optical powers emitted from the selected and non-selected windows.

## III. LED-based optical neural implants

Although lasers and laser diodes provide several benefits, including high light intensity, low beam divergence, and narrow spectral bandwidth, laser-based optical systems have the following drawbacks. First, lasers are power hungry with typical power consumption of several tens of mW per channel. Second, when used with freely behaving animals, lasers require the use of tethered optical fibers and commutation systems, which greatly restrict the natural behavior of the

subjects, require costly optical commutators, and may bias the outcomes.<sup>61</sup> Third, the activation of laser diodes may require relatively high voltage/current, and the possibility of localized heat generation may damage surrounding tissue.

Other disadvantages of laser systems include high cost, mechanical rigidity, unstable illumination, limited precision of analog modulation, and long warm-up times for operation. Compared to laser and laser diodes, LEDs provide unique advantages, including low power consumption, illumination stability, and fast light-switching ability.<sup>62</sup> More importantly, electronically driven LEDs are particularly suitable for integration with wireless telemetries to enable fully implantable systems for applications in freely behaving animals.<sup>63</sup>

The first attempts to use LED light sources for optogenetic neuromodulation were based on commercial packaged bulk LEDs.<sup>61,64,65</sup> Although experiments confirmed the capability of using these packaged LEDs to evoke opsin-expressing cells *in vitro*, the bulky size of the package limits the stimulation resolution and impedes their use for further *in vivo* study. To solve this issue, microfabrication technology has been introduced for processing and packaging μLEDs with very compact size, high spatial resolution, low power consumption, and high illumination. Both custom-designed GaN μLEDs and commercially available μLED chips have been utilized.

For custom-designed GaN μLEDs, dedicated etching and dic-ing processes are required to achieve the desired chip dimensions. A variety of μLED processing approaches have been developed by many researchers, such as Chan-Wook Jeon *et al.*,<sup>66</sup> Haoxiang Zhang *et al.*,<sup>67</sup> and Tae-il Kim *et al.*<sup>68</sup> The fabrication of μLED-coupled optical probes relies on two basic stereotypes of neural probes being used for electrical stimulation: Utah type<sup>69</sup> and Michigan type.<sup>54</sup> In the following sections, the device configurations and fabrication techniques of different μLED-coupled optical neural interfaces are discussed in detail. Representative prototypes are presented in Fig. 2 and their specifications are summarized in Table 2.

### 3.1 Utah-type optical arrays

The Utah neural probes, which were made by bulk micro-machining thick boron-doped silicon substrates, have been widely used for electrical stimulation and chronic neural recordings.<sup>70,71</sup> Compared with the Michigan probe, the Utah probe topology enables the arrangement of high-density shanks in a 3D configuration. Taking this advantage, the Utah probe topology has been adopted to make LED-coupled optical probes for optogenetic applications. The two main

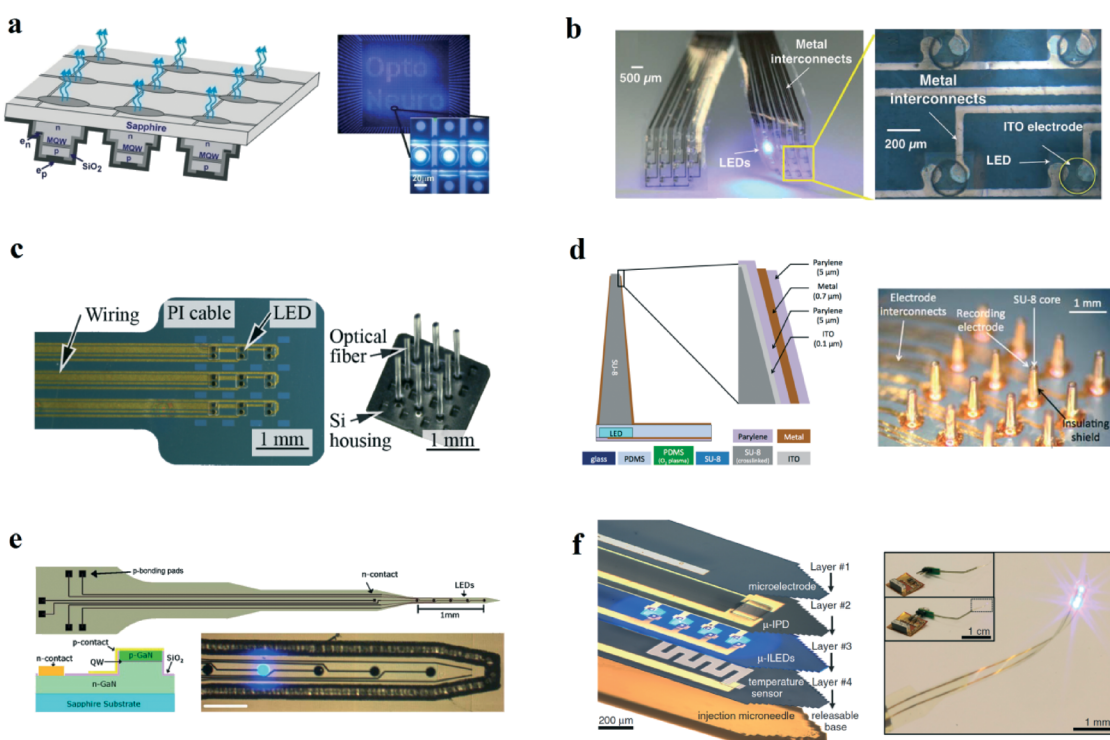


**Fig. 2** Examples of μLED-based neural interfaces. (a) A high-density μLED array fabricated by conventional silicon-based microfabrication technology. Reprinted from ref. 73. (b) A  $4 \times 4$  Opto-μECOG array with a transparent microelectrode array and a μLED array on a flexible Parylene-C substrate for epidural optical stimulation and electrical recording of cortical activity. Reprinted from ref. 78. (c) A μLED-coupled optical fiber array with a miniaturized Si housing plate for optical fiber alignment and fixation. Reprinted from ref. 80. (d) A μLED-coupled SU-8 microwaveguide array fabricated by a droplet backside exposure method, where an ITO-Parylene-gold-Parylene sandwich clay was used to minimize light-induced artifacts. Reprinted from ref. 81. (e) A custom-designed μLED probe fabricated from an epitaxial GaN/sapphire substrate by semiconductor-based micro-fabrication technology. Reprinted from ref. 91. (f) A flexible, multifunctional neural probe with integrated temperature sensor, neural recording electrodes, light intensity sensor, and μLED. Reprinted from ref. 93.

**Table 2** Summary of the specification of miniaturized,  $\mu$ LED-based optogenetic neural implants

Optical neurostimulation components				Electrical recording components					
Light source	# of channels	Dimensions	Output light intensity/energy (max. or used in test)	Light delivery efficiency	# of channels	Dimensions	1 kHz impedance	In vivo or in vitro validation	Ref.
$\mu$ LED-coupled optic fiber	3 × 3	5 mm long, 105 $\mu$ m in diameter, 550 $\mu$ m separation	1.28 mW mm <sup>-2</sup>	-20.56 to -18.97 dB	0	—	—	None	79
$\mu$ LED-coupled optic probe	32	Base size: 300 $\mu$ m, tip size: 30 $\mu$ m	10 mW mm <sup>-2</sup>	-10 dB	32	Electrode size: 30 $\mu$ m	10–500 k $\Omega$	<i>In vivo</i>	81
Surface-mounted $\mu$ LED array	64 × 64	20 $\mu$ m in diameter 50 $\mu$ m separation	250 mW mm <sup>-2</sup>	—	0	—	—	<i>In vitro</i>	73
Surface-mounted $\mu$ LED array	3	200 $\mu$ m in diameter, 700 $\mu$ m separation	10 mW mm <sup>-2</sup>	—	16	200 $\mu$ m in diameter, 700 $\mu$ m separation	1–5 k $\Omega$	<i>In vivo</i>	78
Penetrating probe with $\mu$ LED	5 × 1	1.3 mm long, 80 $\mu$ m wide, $\mu$ LED diameter: 40 $\mu$ m, 250 $\mu$ m separation	600 mW mm <sup>-2</sup>	2%	0	—	—	None	91
Penetrating probe with $\mu$ LED	1	12 mm long, 900 $\mu$ m wide, $\mu$ LED: 1 × 0.6 × 0.2 mm <sup>3</sup>	0.7 mW mm <sup>-2</sup>	—	3	50 $\mu$ m × 100 $\mu$ m	—	<i>In vivo</i>	89
Penetrating probe with $\mu$ LED	1	4.2 mm × 0.86 mm × 0.28 mm, $\mu$ LED: 0.55 mm × 0.29 mm × 0.1 mm	1 mW mm <sup>-2</sup>	—	0	—	—	<i>In vivo</i>	90
Penetrating probe with $\mu$ LED	1	~400 $\mu$ m wide, 20 $\mu$ m thick, $\mu$ LED: 50 mm × 50 mm × 6.45 $\mu$ m	7–17.7 mW mm <sup>-2</sup>	—	1	20 $\mu$ m × 20 $\mu$ m	1 M $\Omega$	<i>In vivo</i>	93
Penetrating probe with $\mu$ LED	2	8 mm × 6.8 mm × 0.25 mm, $\mu$ LED: 0.55 mm × 0.29 mm × 0.1 mm	1.5 mW mm <sup>-2</sup>	—	4	120 $\mu$ m in diameter	20–90 k $\Omega$	<i>In vivo</i>	103

designs of Utah-type optical probes include planar, surface-mounted LED arrays and 3D arrays with  $\mu$ LEDs coupled to optical fibers or waveguides. Probes based on the former design are primarily used in *in vitro* studies with cell culture and brain slice preparations, while the latter design targets *in vivo* studies in the deep cortical layers and brain regions of living animals. The following two sections will discuss in more detail the surface-mounted  $\mu$ LED arrays and optical fiber/waveguide-coupled  $\mu$ LEDs array.

**3.1.1 Surface-mounted  $\mu$ LED arrays.** Nir Grossman *et al.*<sup>66,72–74</sup> (Fig. 2(a)) used conventional silicon-based micro-fabrication technology to build the first custom-designed, high-power  $\mu$ LED array, which can generate arbitrary optical excitation patterns with micrometer and millisecond resolution. Despite the successful demonstration of optical modulation of neural activity with high density and high spatial resolution, this type of probe suffers from disadvantages related to the integration of neural recording capability and heat generation due to high-density  $\mu$ LED illumination. In their *in vitro* study, because a whole-cell patch clamp was used for neural signal recording, it was difficult to record signals from multiple neurons simultaneously. In addition, these  $\mu$ LED arrays would have difficulties in thermal management, especially when operated at high frequency and long duration, due to their ultra-high density (a 64 × 64  $\mu$ LED array with a small pitch of 50  $\mu$ m). The excessive heating may cause tissue damage as well as physiological and behavioral change,<sup>75</sup> which may bias the outcomes of optogenetics.

Besides custom-made  $\mu$ LED arrays, commercially available die-form LED chips are employed in the fabrication of surface-mounted optical arrays because of their compact size, high power efficiency, and low cost. Die-form  $\mu$ LED chips are available through several manufacturers, such as Samsung Inc., Cree, and Rohm Semiconductor. Polymers, such as Parylene-C, SU-8 and polyimide,<sup>76</sup> have been used as carrying substrates and insulating layers of the LED chips due to the mechanical flexibility, biocompatibility, chemical resistance, and stability of the polymers. As an example, Ki-Yong Kwon *et al.*<sup>77,78</sup> (Fig. 2(b)) reported a multichannel Opto- $\mu$ ECoG array, which combines a transparent microelectrode array and a  $\mu$ LED array on a flexible Parylene-C substrate for epidural optical stimulation and electrical recording of cortical activity. The  $\mu$ ECoG array featured a Parylene-indium tin oxide (ITO)-gold-Parylene sandwich structure for electrical recording without compromising the optical throughput. Self-assembly of commercially available  $\mu$ LED chips (220  $\mu$ m × 270  $\mu$ m × 50  $\mu$ m, Cree TR2227TM) was achieved by pre-aligning the chips onto a Parylene substrate with patterned metal interconnects followed by bonding the LEDs to the matched contact pads using low melting point solder in a hot acid bath. The  $\mu$ ECoG array and the  $\mu$ LED array were fabricated separately and then aligned and bonded together using adhesive polymers. The optical stimulation of opsins-expressing cortical neurons was confirmed *in vivo* by observing light-evoked ECoG signals recorded through the ITO microelectrodes and action potentials recorded through a

carbon fiber probe. It is of note that the maximum temperature variance of this device was  $\sim 9$  °C and  $\sim 1$  °C when the LED was driven by 100 ms voltage pulses of 3.2 V and 2.7 V, respectively. Hence, the application of this probe is limited to short pulses with low applied voltage.

**3.2.2 Optical fiber/waveguide-coupled  $\mu$ LED arrays.** The surface-mounted  $\mu$ LED arrays have limited stimulation depths due to the scattering and absorption of LED light by neural tissue.<sup>75</sup> In view of such shortcomings, significant developments have been made to couple  $\mu$ LED light into waveguiding structures, such as optical fibers, micro-waveguides, and optrodes, for delivering light into deep brain regions. For example, a  $3 \times 3$ , LED-coupled, optical fiber array was reported by Michael Schwaerzle *et al.*<sup>79,80</sup> (Fig. 2(c)). In this design, commercially available  $\mu$ LED chips ( $270 \mu\text{m} \times 220 \mu\text{m} \times 50 \mu\text{m}$ , Cree C460TR2227-S2100) were flip-chip bonded onto a polyimide substrate with patterned metal interconnects. DRIE was used to machine a miniaturized Si housing plate that carried the  $\mu$ LED chips and aligned them to optical fibers with high precision. The equivalent coupling efficiency between LEDs and fibers was measured to be  $\sim 0.88\text{--}1.27\%$ . When the LEDs were driven by 30 mA current pulses, the maximum temperature variations on the silicon housing were 5, 10, and 15 °C with 5%, 10% and 15% pulse duty cycles, respectively. Although this device allows light delivery into deep cortical areas, the commercially available optical fibers are still bulky and have few tip-size options, resulting in low spatial resolution. In addition, each optic fiber was assembled to its base manually, which will be very labor-intensive and costly for batch fabrication.

Recently, LED-coupled SU-8 microwave guide arrays have been developed by Ki-Yong Kwon *et al.*<sup>81 $\text{--}$ 87</sup> (Fig. 2(d)) using polymer-based MEMS techniques. These 3D arrays were equipped with single-length or varying-length slanted micro-waveguides to deliver light to the same or different layers of the cortex. Backside UV exposure of an SU-8 photoresist was used to create taper-shaped waveguides with the tip and base diameters controlled by adjusting the mask designs and the separation between the mask and the resist layer. To monolithically pattern varying-length waveguides on a single substrate, a droplet backside exposure (DBE) method was introduced, where the length variation of the waveguides was achieved by manipulating the shape of an SU-8 droplet dispensed on a plasma-treated polymer substrate. Building on the 3D waveguide arrays, an ITO-Parylene-gold-Parylene sandwich clay was coated on the outer sidewalls of the SU-8 waveguides to serve several functions. In particular, the ITO layer was used to eliminate photoelectrical artifacts without compromising the light transmission. The opaque gold layer was used to block out the light leakage and record light-evoked neural activity. The Parylene was used as the electrical insulator and the packaging coating. The light intensity was  $\sim 1 \text{ mW mm}^{-2}$  with an applied voltage of 2.7 V, and  $\sim 10 \text{ mW mm}^{-2}$  with an applied voltage of 2.9 V, measured from the tip of the microwave guide, showing that sufficient light can be delivered through the SU-8 microwave guides. The

coupling efficiency was estimated to be  $\sim 10\%$ , which is close to the maximum coupling efficiency of LED-fiber butt-coupling.<sup>88</sup> The maximum temperature variation of the LED was  $\sim 9$  °C with an applied voltage of 3.2 V and 100 ms activation duration.

While the above fiber/waveguide-coupled  $\mu$ LED arrays have been successfully tested *in vivo*, the main limitation of these devices is the low efficiency of the LED-fiber butt coupling, which is typically less than 10%. In order to maintain sufficient light intensity for effective photostimulation of opsins, high applied voltage and long duration of driving pulses are necessary, which will inevitably increase the local temperature. The low thermal conductivity of the polymer substrate and package also prevents heat transfer from the devices to the surrounding biological environment, therefore increasing the risk of thermally induced tissue damage.

### 3.2 Michigan-type optical probes

In order to achieve highly efficient light coupling, an alternative light delivery strategy has been explored by inserting  $\mu$ LEDs directly into deep brain targets of interest. Well-established Michigan-type probes provide an ideal platform where both custom-designed and commercially available  $\mu$ LED chips can be mounted onto the probe tip as light sources for optical neuromodulation. Michigan-type optical probes constructed with commercial  $\mu$ LED chips have been reported by many research groups. As an example, Hung Cao *et al.*<sup>89</sup> developed a hybrid optical/electrical probe with one stimulating  $\mu$ LED and three recording microelectrodes integrated on a 12 mm-long and 900  $\mu\text{m}$ -wide polyimide probe shaft. The  $\mu$ LED ( $1000 \mu\text{m} \times 600 \mu\text{m} \times 200 \mu\text{m}$ , Pico LED, Rohm Semiconductor, Kyoto, Japan) was coupled to a polymerized lens for collimating divergent light from the  $\mu$ LED. As another example, Bin Fan *et al.*<sup>90</sup> recently reported an SU-8 optical probe, where an SU-8-metal-SU-8 sandwich structure was used to encapsulate a Samsung  $\mu$ LED ( $550 \mu\text{m} \times 290 \mu\text{m} \times 100 \mu\text{m}$ ) and its electrical interconnects. The probe shaft was 4.2 mm long and 860  $\mu\text{m}$  wide, capable of stimulating neurons in deep brain regions.

Although using commercially available  $\mu$ LED chips can reduce the complexity of device fabrication and  $\mu$ LED assembly, the dimensions of  $\mu$ LEDs are limited by factory specifications, which makes it difficult to miniaturize the devices. A custom-designed  $\mu$ LED chip will provide an opportunity for the miniaturization of Michigan-type probes to increase the spatial resolution of photostimulation, reduce device invasiveness, and prevent unnecessary tissue damage. Both semiconductor-based and polymer-based microfabrication technologies have been explored. A representative prototype built using traditional semiconductor technology was reported by Niall McAlinden *et al.*<sup>91,92</sup> (Fig. 2(e)). In this case, a blue  $\mu$ LED probe was fabricated from a commercial LED wafer with epitaxial GaN structures grown on a sapphire substrate. A 7 mm-long probe carried five LEDs (with a diameter of 40  $\mu\text{m}$  and a pitch of 250  $\mu\text{m}$ ) on a 1.3 mm-long tip shaft

for optical neuromodulation. Laser dicing was used to shape the sapphire probe followed by mechanical thinning of the probe to 100  $\mu\text{m}$  thick from the backside of the substrate. With a 200 ms driving pulse (resulting in 600 mW  $\text{mm}^{-2}$  light intensity), the probe had a maximum temperature rise of less than 2  $^{\circ}\text{C}$ , which benefits from the relative high thermal conductivity of sapphire ( $23 \text{ W m}^{-1} \text{ }^{\circ}\text{C}^{-1}$ ). Despite the low heating benefit, this device suffers from the mechanical rigidity of sapphire, which may promote a neuro-inflammatory response, induce mechanical strains in the surrounding tissue, and lead to irreversible tissue damage during chronic applications in freely moving subjects.

As a solution, mechanically compliant polymeric substrates can be used to carry the LEDs. However, most fabrication processes for making inorganic LEDs, particularly for blue GaN LEDs, are incompatible with polymers, due to the requirement of high processing temperatures. Therefore, novel techniques are needed to transfer pre-fabricated  $\mu$ LED chips from a solid substrate (sapphire or silicon carbide) to a flexible polymer substrate. Tae-il Kim *et al.*<sup>68</sup> demonstrated a  $\mu$ LED substrate transfer technology, by which  $\mu$ LEDs with lateral dimensions ranging from 1 mm  $\times$  1 mm to 25  $\mu\text{m}$   $\times$  25  $\mu\text{m}$  can be transferred from a foreign substrate such as sapphire to a target polymer substrate. Using this technology, Tae-il Kim *et al.*<sup>93</sup> (Fig. 2(f)) implemented a flexible, multifunctional, neural interface probe, which consisted of a platinum microelectrode array for neurophysiological recording, a  $\mu$ LED array for optical neuromodulation, a precision temperature microsensor layer for real-time monitoring of local temperature variation, and a microscale, ultrathin silicon photodiode array for measuring the light intensity of  $\mu$ LEDs. Each sensor/array layer was constructed on a flexible polyester substrate and then stacked and bonded together with UV-curable epoxy. A releasable base was fabricated from epoxy and bonded to the as-fabricated hybrid neural probe with bio-resolvable adhesive silk to facilitate the insertion of the mechanically flexible probe into brain tissue. Such multifunctional devices can be powered wirelessly using a radio-frequency (RF) transmitter and a signal generator for experiments with freely moving animals. The devices were tested *in vivo* to demonstrate their functionalities for optical stimulation, electrical recording, and dissecting complex neurobiology and behavior of freely moving animals. The time-average temperature change with various duty cycles at 17.7 mW  $\text{mm}^{-2}$  peak light output was within 1  $^{\circ}\text{C}$  when the device was inserted 0.3 mm into brain tissue. As the state of the art, these multifunctional optoelectronics present significant advantages, including spatially precise and cellular-scale light delivery, highly effective thermal management, mechanical flexibility, and integration with wireless components to eliminate the need for fiber optics, tethers, and commutators. While such devices have shown great improvements over the previous instruments, they are not without significant concerns. These include potential thermally induced tissue damage due to LED heat deposition in the brain as well as electronic failure, particularly for high-density neural

implants where microelectronics are in direct contact with large-area brain tissues. Furthermore, the very limited adaptation of this exciting method by other researchers in this field could be mainly due to the labor-intensive and costly process of device fabrication.

## IV. Miniaturized, wireless optical neural implants

Long-term behavior study in freely behaving animals requires untethered, fully implanted neural interfaces with real-time neural recording and closed-loop optical stimulation capabilities, which can reduce the risk of inflammation due to the wire connections and facilitate the control of multiple study subjects without tangling wires.<sup>14</sup> To meet this critical need, several attempts have been made to construct wirelessly powered and controlled optical neural implants, which can be categorized based on battery-needed and battery-free system architectures. Fig. 3 provides several examples of wireless optogenetic stimulators. More details of system configurations and characteristics are discussed below.

### 4.1 Battery-powered optical neural implants

This section will discuss the examples of battery-powered optical implants. In one example,<sup>94</sup> a rechargeable lithium polymer battery was used to drive a low-power, microcontroller-based optical stimulator (Fig. 3(a)). A Gaussian frequency-shift keying transceiver was used to communicate wirelessly with a host computer at 2.4–2.5 GHz within 4 m. The digital-to-analog converter (DAC) of the microcontroller was connected to a driver circuit for powering two  $\mu$ LEDs with constant current, resulting in the output light power of up to 32 mW. The battery was able to last over 2 h with a single recharging time of 20 min. The overall microsystem printed circuit board had a light weight of 2.9 g and a small form-factor of 14 mm  $\times$  17 mm  $\times$  5 mm, which is suitable for applications in small, freely behaving animals.

Another example is an LED stimulator based on infrared (IR) interrogation.<sup>95</sup> In this device, different stimulation parameters were digitalized into an 8-bit binary code, which was then transmitted using amplitude-shift keying (ASK) with a carrier frequency of 38 KHz, through IR-LEDs of a microcontroller, to an IR receiver mounted on an implanted headstage. These signals were used to selectively drive a 4-channel LED array with the output light intensity of up to 4.6–6.07 mW  $\text{mm}^{-2}$ . The communication range between the IR transmitter and the receiver was 15 m long. The microcontroller on the headstage was powered by a 3.7 V lithium polymer battery with a boost converter to 5 V. The standby time and driving time of this LED stimulator were 3.5 h and 67 min, respectively, under the stimulation parameters of 50 ms pulses at 10 Hz for 2 s duration and 5 s intervals. The overall weight of the headstage with the battery was 2.4 g and the total dimension was 14 mm  $\times$  14 mm  $\times$  10 mm.

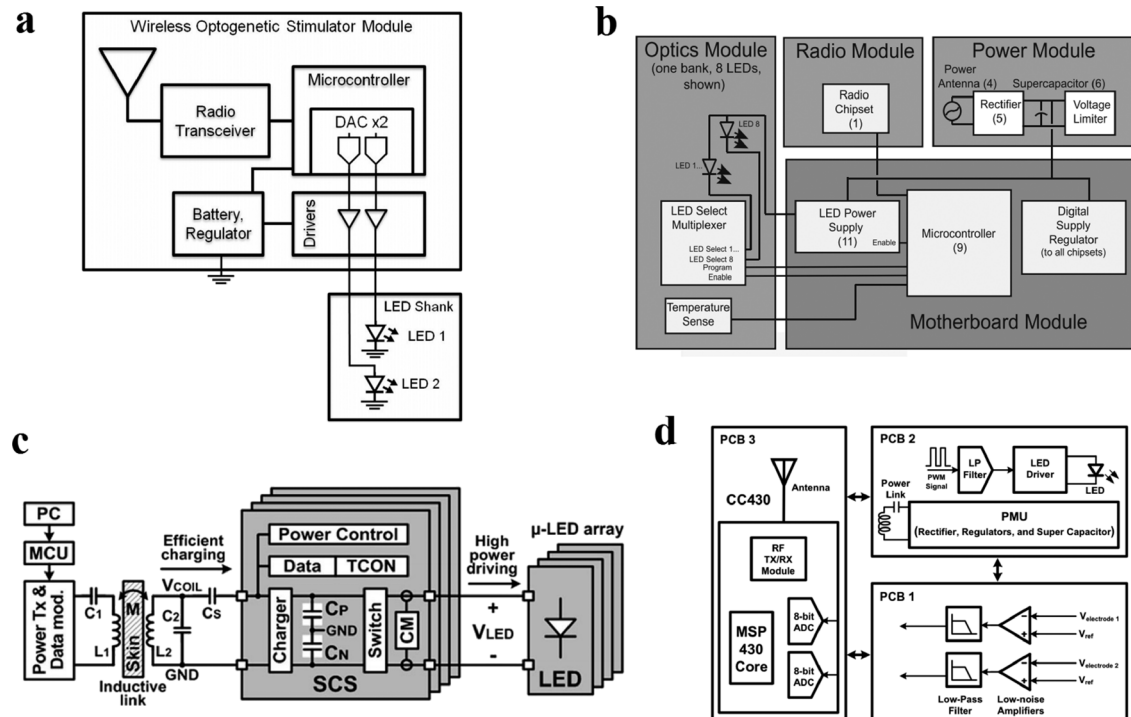


**Fig. 3** Block diagrams of several wireless optogenetic stimulators. (a) A microcontroller-based optical stimulator driven by a battery. Reprinted from ref. 94. (b) A wireless optical neural implant controlled by a microcontroller, which was powered by a wirelessly charged supercapacitor. Reprinted from ref. 97. (c) A simplified block diagram of a wireless, battery-free SCS system. Reprinted from ref. 81. (d) A dual-modal microcontroller-based neural interface powered by a wirelessly charged supercapacitor, for optical stimulation and neural recording. Reprinted from ref. 98.

Recently, Steven Lee *et al.*<sup>96</sup> implemented an optogenetic stimulator in a similar configuration, which consisted of a cranially mounted fiber-coupled LED for photostimulation, a microcontroller to control stimulation parameters, a wireless link for triggering stimulation, and rechargeable solid-state batteries for supplying power. The device, with a volume size of 12 mm × 7 mm × 11 mm and total weight of less than 1.6 g, was validated *in vivo* using freely moving and unrestricted mice.

The battery-powered optical stimulator provides a simple and straightforward method to deliver light into the brain wirelessly. However, several considerations must be taken into account. On the one hand, the overall weight of the headstage should be minimized to prevent interference with the free movement of subjects. A trade-off between the overall weight of the headstage and the capacity of the battery should be considered in the design of such systems. Generally speaking, the more capacity a battery has, the more it weighs. On the other hand, given a fixed battery capacity, a compromise has to be made between stimulation intensity and operational time, which limits the applications of such battery-powered neural implants.

#### 4.2 Battery-free optical neural implants

In order to address these issues, wireless power telemtries have recently been studied and integrated with optical neural implants. Wireless power transfer can be achieved either by

inductive coupling through a pair of coils resonating at the same frequency or by RF scavenging that transfers microwave energy from a transmitter antenna to a receiver antenna for powering electronic components. Several representative prototypes of miniaturized, wirelessly powered optical neural implants are introduced below.

An inductively powered optical stimulator was reported in<sup>97</sup> where power was transmitted through an inductively coupled telemetry link and restored in a supercapacitor (Fig. 3(b)). Optical stimulation was wirelessly controlled by a microcontroller, which was powered by the supercapacitor through a full-wave rectifier and communicated with a host computer through a 2.4–2.485 GHz surface-mounted antenna. The overall headstage weighed 3 g, had a compact volume size of <1 cm<sup>3</sup>, and was able to deliver 2 W power (maximum 4.3 W with a reduced duty cycle) to 16 LEDs.

Most recently, a wireless neural interface consisting of multimodal optical stimulation and neural recording elements was reported by Reza Ameli *et al.*<sup>98</sup> (Fig. 3(d)). In this system, a 4-coil inductive link was used to deliver power wirelessly for driving an LED with a constant current of 5–9 mA and for charging a supercapacitor that served as the power source of the whole headstage. Photostimulation was controlled at a back-end station through RF telemetry. Recorded neural signals were first amplified by a low-noise amplifier, conditioned by a low-pass filter, and then converted into digital signals by an 8-bit analog-to-digital converter (ADC). Then the digital signals were transmitted to the back-end station

through an RF microcontroller with a data rate of up to 320 kbit s<sup>-1</sup>. This device had a footprint of 15 mm × 25 mm × 17 mm, weighed 7.4 g, and had a data transmission range of over 2 meters.

The aforementioned wireless systems are normally constructed by populating discrete electronic components with printed circuit boards (PCBs). For the further miniaturization of wireless optical systems, a wirelessly powered, switch-capacitor-based stimulating (SCS) application-specific integrated circuit (ASIC) was designed and implemented by Hyung-Min Lee *et al.*<sup>81,83</sup> (Fig. 3(c)). The SCS system efficiently charged a bank of storage capacitors directly through a resonant inductive link without using any rectifiers or regulators. The charge stored in the capacitors was able to drive four μLEDs using decaying exponential pulses with a high stimulation efficiency of 80.4%. *In vivo* testing demonstrated the capability of this integrated wireless system for recording light-induced local-field potential changes.

As an alternative solution to resonant inductive coupling, an RF power-scavenging module was reported in.<sup>93</sup> The transceiver module consisted of an RF signal generator, an RF power amplifier, and an RF antenna for broadcasting at 910 MHz. The headstage combined a receiver panel antenna, an impedance coupling network, a rectifier, and a voltage multiplexer on a compact platform, which can efficiently drive μLEDs with the output power density of up to 7 mW mm<sup>-2</sup>. The power density of microwave radiation at a distance of 1 m was measured within the maximum permissible exposure limit of 3.03 mW cm<sup>-2</sup>. The total weight of the headstage was around 2.7 g, including a polyimide-based optoelectronic probe and printed circuit boards.

While both the resonant inductive coupling and the RF scavenging show promise for the development of wirelessly powered optical neural implants, some technical challenges still remain unsolved. First, most of the current systems mainly focus on wirelessly controlled optical stimulation, except the system described in,<sup>98</sup> whose efficacy has not yet been validated *in vivo*. Second, the output power density of light is limited to a few mW mm<sup>-2</sup>, which may not be sufficient for certain applications, such as behavior change studies. Third, due to environmental interferences, such as animal movement, and the interference between power and data transmission antennas, it is difficult to recover high signal-to-noise-ratio recording data from the back telemetry. Finally, the levels of microwave and magnetic field radiations should be carefully monitored and tuned within the maximum exposure range to prevent unwanted heating of brain tissue due to the absorption of electromagnetic energy by tissues.

## V. Challenges and discussions

As optogenetic studies have rapidly expanded into *in vivo* applications using freely moving animals, there is an increasing demand for the development of untethered optical tools for wirelessly controlled optical stimulation and neural readouts of large-scale brain circuitry. Two major types of optical

microdevices based on laser and LED light sources have been surveyed in this paper. Compared to bulky and tethered laser systems, μLED-based optical neural implants are favored for their relatively smaller size, higher light coupling efficiency, multiple modalities, and capability of being integrated with wireless power/data telemtries (Fig. 4). Despite the significant development of a wide variety of μLED-based devices, several challenges still remain: localized heating due to LED activation, light-induced artifacts, material compatibility and safety, and complicated device fabrication. The following sections discuss these challenges in the current approaches and envision possible solutions to the identified problems.

### 5.1 Thermal challenges of putting μLED near tissue

To prevent tissue damage and consequent behavioral and physiological changes, the temperature perturbation induced by optical neural implants should be less than 1 °C.<sup>99,100</sup> Therefore, several important considerations should be taken into account when designing LED-based optical devices. First, device layout and μLED array configuration can be optimized to minimize electrical heat generated from μLEDs. Second, the proper selection of substrate materials can potentially reduce localized heating effects by dissipating the LED heat into surrounding brain tissue. The high thermal capacity of brain tissue as well as the circulation of body fluids can counteract the temperature variation. Third, optical stimulation parameters should be optimized to enable effective

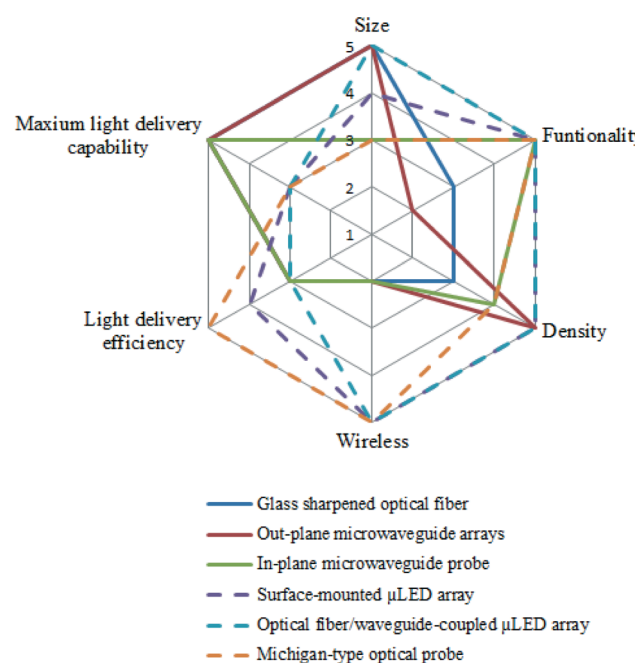


Fig. 4 A spider schematic compares several main specifications of the laser- and LED-based microdevices surveyed in this paper in terms of size, density, multiple functions, wireless capability, light delivery efficiency, and maximum light delivery capability. The performance is rated on a scale of 1 to 5, with 5 being the best.

opsin activation while preventing the overheating of brain tissue.

In order to reduce electrical heat generated during the operation of  $\mu$ LEDs, the thermal performance of  $\mu$ LEDs has been explored analytically and experimentally.<sup>68,93,101,102</sup> LEDs with different dimensions were fabricated<sup>68</sup> on a poly(ethylene terephthalate) (PET) substrate. The thermal performance was quantified by measuring the maximum temperature change upon activating the LEDs under different conditions using a thermal imager. The following findings are derived from these studies. First, increasing the LED size can lead to an increase in the maximum temperature change and a decrease in the overall energy efficiency. Second, when designed in an array configuration, increasing the separation between  $\mu$ LEDs can effectively decrease the maximum temperature change. Finally, decreasing the pulse duty cycle can also reduce the maximum temperature rise.

In addition, analytical and finite element method (FEM) simulations<sup>101</sup> have been conducted to predict the thermal behavior of  $\mu$ LEDs and  $\mu$ LED arrays in tissues. Both approaches imply that the maximum temperature change in tissues can be reduced by lowering the peak power and decreasing the duty cycle and period of LED activation. For a  $\mu$ LED array, a larger  $r_d / \sqrt{A}$  will result in a smaller temperature change, where  $r_d$  is the distance between the centers of two adjacent  $\mu$ LEDs and  $A$  is the total surface area of the  $\mu$ LED.

To further reduce the temperature variation during optical stimulation, especially the localized hot spots, a substrate material with high thermal conductivity should be carefully selected. Recently,  $\mu$ LED probes made of polycrystalline diamond (PCD) were reported by Bin Fan *et al.*,<sup>103</sup> where polycrystalline diamond was utilized as a heat spreader, taking advantage of its high thermal conductivity (up to 2000 W (m<sup>-1</sup> K<sup>-1</sup>)).<sup>104</sup> With various input pulses, the local temperature variation of the PCD probes can be suppressed within 1 °C, as compared to ~9 °C for an SU-8 probe (with a thermal conductivity of 0.3 W (m<sup>-1</sup> K<sup>-1</sup>)). Besides, PCD has a unique combination of properties, making it a promising material for the development of next-generation implantable neural interfaces. Among the favorable properties are electrical insulation, chemical inertness, high resistance to surface fouling, and biocompatibility.<sup>105,106</sup>

## 5.2 Light-induced artifacts

For hybrid optoelectronic implants used in simultaneous recording of light-evoked neural activity, low-frequency voltage swings or artifactual spikes were observed from local field potentials or action potentials when microelectrodes were exposed to illumination.<sup>32,107,108</sup> Such light-induced artifacts present as voltage ramping aligned with the onset of light illumination or slow voltage discharging,<sup>32</sup> with amplitudes proportional to illumination power. Such light-induced artifacts can be caused by a photoelectric effect and a photoelectrochemical effect (known as the Becquerel effect<sup>109</sup>). The

photoelectric effect is commonly seen in semiconducting materials that have an energy gap below the photo energy of visible light (~3.1–1.8 eV), such as silicon. For conducting materials, the Becquerel effect is likely to be the main contributor of light-induced artifacts and can be caused by the transfer of photon-excited charges across the ionic charge layer at the electrode–electrolyte interface.<sup>110</sup> When conventional metal electrodes are placed in an electrolyte (*e.g.* saline), light-induced artifacts caused by the Becquerel effect are difficult to prevent and can obscure neural recording signals.

Engineering solutions have been explored to reduce light-induced artifacts. One approach is to reduce the metal area of the recording electrodes or wires exposed to the light sources. This is typically used in optical systems based on laser-coupled optical fibers, where a separate set of recording electrodes can be employed to record light-evoked neural responses. For example, it has been demonstrated that using thin tungsten wire sterotrodes with a wire diameter of <20  $\mu$ m and coating glass electrodes with non-reflective materials can significantly reduce or eliminate optical artifacts.<sup>32</sup> It has also been found that changing the angle between the laser beam and the recording metal electrode can help reduce photoelectric artifacts.<sup>32,109</sup>

Another way of reducing light-induced artifacts is to replace conventional metal materials (*e.g.* gold and platinum) with conducting thin-film materials that are more resistant to the Becquerel effect. Some transparent conducting materials, such as ITO and graphene, have been investigated in order to suppress the photocurrent while providing sufficient conductivity for effective neural recording. The first reported ITO microelectrode interface was developed by Anthony N. Zorzos *et al.*,<sup>111</sup> where nichrome (NiCr) wire was dipped in an ITO nanoparticle solution followed by sintering at 50 °C for 30 minutes in air. The ITO-coated NiCr wires resulted in significant reduction in photoelectrochemical artifacts, which was ten times lower than that of normal NiCr wires. Another example of using ITO in the fabrication of  $\mu$ LED-based optrodes was reported by Ki-Yong Kwon *et al.*<sup>86</sup> In this case, an ITO–Parylene–gold–Parylene sandwich clay was constructed on the outer sidewalls of the SU-8 waveguide, and wires were connected to the ITO layer to ground the photocurrent induced by LED illumination. Most recently, Dong-Wook Park *et al.*<sup>112</sup> reported that photoelectric artifacts can be effectively reduced by utilizing highly conductive graphene-based carbon<sup>112</sup> as the transparent electrodes during optogenetic neuromodulation.

## 5.3 Material long-term compatibility and safety

One of the major challenges of fiber- or waveguide-coupled optical systems is to obtain high optical transmission efficiency from the fiber (or waveguide) to the stimulation site. As discussed in the previous sections, microfabricated fibers and waveguides are normally made of polymers, such as SU-8, or dielectric materials, such as oxynitride. While polymers

provide excellent mechanical flexibility and fabrication simplicity, the absorption of water could negatively affect the long-term optical properties of the polymer-based devices. Deterioration of mechanical properties of polymer waveguides is also observed during aging of the devices in buffered saline solution (PBS). Moreover, commonly used photo-sensitive polymers, such as SU-8, have a high absorption loss near 473 nm,<sup>113,114</sup> which significantly reduces their light-guiding quality. Finally, the biocompatibility of SU-8 has not been fully evaluated in chronic studies. Dielectric materials are considered to be more appropriate than polymers because of their biocompatibility, low water permeation and absorption rates, and optical clarity over a broad spectral region. However, thick dielectric waveguides are difficult to construct due to stress and extended plasma etching time. As a result, the coupling efficiency between thin dielectric waveguides and multi-mode fiber optics can be significantly affected by the large coupling loss at the fiber-waveguide junction. Further modification and optimization of fabrication techniques are necessary to improve the coupling efficiency. Furthermore, silicon-based dielectric films have shown increased dissolution in water at elevated temperatures and may require additional encapsulating barriers for chronic applications.<sup>115</sup>

Another major challenge of chronic neural implants is the mechanical property mismatch between rigid implanted devices and soft brain tissue, which increases the possibility of negative neural response, glial scar formation, inflammation, and mechanically induced trauma.<sup>116–118</sup> While the mechanical rigidity can be alleviated by the use of polymer substrates, the surgical insertion of such flexible devices into deep brain regions will be challenging. To address this issue, a temporary coating that can stiffen the probe during the insertion and be dissolved by body fluids afterwards has been adopted to facilitate the implantation of the flexible optical neural implants. Among different biodegradable polymers, silk fibroin, a biopolymer obtained from cocoons, has been widely used in bio-integrated electronics.<sup>119</sup> Silk fibroin can be dissolved by most aqueous solutions with a programmable rate of dissolution controlled by the ratio of solvent and silk concentrations. Tae-il Kim *et al.*<sup>93</sup> successfully demonstrated the use of silk to temporarily bond a flexible μLED probe to a thick and rigid epoxy carrier during probe insertion. The silk fully dissolved in an artificial cerebrospinal fluid (ACSF) solution 15 min after the insertion was made. Another dissolvable adhesive, polyethylene glycol (PEG), was used by Falk Barz *et al.*<sup>120</sup> In this study, the PEG with a molecular weight (MW) of 1500 g mol<sup>-1</sup> was quickly dissolved in electrically conducting agar-based gel in 1 min. As the melting point of PEG with different MW can range from 4 to 8 °C (MW = 400) to 55–62 °C (MW = 8000),<sup>121</sup> a careful selection should be conducted to match the temperature range of the target implantation sites.

Furthermore, as implantable devices become miniaturized, the amount of water needed to increase the humidity of the encapsulated environment decreases accordingly, which

takes a shorter time for implanted materials to reach corrosive levels.<sup>122</sup> Therefore, encapsulating materials and techniques should be carefully considered in order to achieve long-term stability of implantable devices. Although traditional processes such as glass-to-metal seal, ceramic-to-metal seal, and fusion welding can provide real hermetic sealing for implantable devices, the high processing temperature may not be compatible with polymer-based implantable devices. Recently, polymer encapsulations, such as Parylene, polyimide, silicone and epoxy, have been widely used as a barrier coating for electronics. Although the biostability of these materials is questionable because polymers tend to degrade due to hydrolytic, oxidative, and enzymatic mechanisms,<sup>123</sup> recent studies have shown that Parylene encapsulation of CMOS circuitry can survive at 55 °C for 5 months. Besides, metal-coated Parylene barriers may further reduce the permeability of moisture and can remain intact *in vivo* for over 10 years.<sup>124</sup> Atomic-layer-deposited alumina-Parylene bilayer encapsulation has also been studied, where a Utah electrode array (UEA) with an ASIC chip survived for 228 days of soaking testing at 37 °C.<sup>125</sup>

Finally, biocompatibility has always been an important criterion of all the implantable devices to prevent glial formation and other foreign body reactions that present significant risks for devices and host tissue. Particularly for optogenetics applications, glial encapsulation can increase the backscattering and attenuate light delivered to host tissue.<sup>126</sup> Common strategies for minimizing foreign body responses include careful selection of biomaterial coatings, surface modification, and optimization of device design to reduce size and mechanical mismatch. Considerable work on biomaterials and biocompatibility issues for neural implants has been compiled in.<sup>76,127,128</sup>

#### 5.4 Fabrication complication of ultracompact μLED arrays

As demonstrated in the previous section, a smaller LED size can improve the spatial resolution of optical stimulation and reduce the heat generation during the activation of μLEDs. As most of the commercially available μLEDs do not have a small enough die size, methods for fabricating custom-designed, ultra-compact μLEDs are needed and usually require expensive and complex processing tools. As an example, a method of transferring a GaN ultra-compact μLED onto a flexible PET substrate was invented by Tae-il Kim *et al.*,<sup>68</sup> where laser lift-off and deterministic assembly methods were employed to prevent the use of wafer dicing and individual μLED pick-and-place assembly. Epitaxial lift-off of the patterned GaN LED structures from the sapphire substrate was achieved by thermal decomposing an undoped GaN sacrificial layer into Ga metal and nitrogen gas, using localized laser heating. This fabrication approach takes advantage of the mature chip-scale semiconductor processing and combines it with patterned interconnects, which enable the release and transfer of ultra-compact LEDs and other electronics fabricated on wafers onto mechanically flexible

polymer substrates (PET, silicone, polyimide, or silk fibroin). However, the fabrication complication may limit the adoption of such methods by other research groups and researchers.

## VI. Conclusion and outlook

Optogenetics, as a new neuromodulation technology, has drawn increasing attention from the neuroscience community due to its cell-type specificity and high spatiotemporal resolution. Reliable light delivery and neural signal readout strategies are needed for studying the relationship between neural activity and behavioral change in freely moving animals. To date, many efforts and attempts have been made, aiming at the engineering development of reliable, implantable, low-power, wireless neural interfaces for optogenetic applications. Ideally, such interfaces should allow delivery of high-intensity light into target cells without causing excessive temperature rises in surrounding biological environment, and bidirectional communication between the implanted device and external electronics for neural signal recording and closed-loop optical stimulation.

Two major types of miniaturized optical neural implants based on laser and LED light sources have been explored extensively: both have advantages and disadvantages. Lasers and laser diodes can provide high light intensity with low beam divergence and narrow spectral bandwidth because of their coherent radiation characteristic. However, the flexibility of applying the laser-based systems to studies in freely moving animals has been limited by the tethered fiber optics and the bulky size of laser sources. Alternatively, micro-fabricated LED-based systems provide many favorable advantages, such as ultra-compact size, mechanical flexibility, high spatial resolution, and wireless capability. However, due to the incoherent radiation of LEDs, the fiber-coupled light delivery approach suffers from the limited coupling efficiency between LED and fiber. Penetrating probes with LEDs coupled directly to targeted neurons are more competitive than the fiber-coupled devices, in terms of coupling efficiency, power consumption, and fabrication simplicity. However, when  $\mu$ LEDs are implanted in brain tissues, Joule heating during the activation of the  $\mu$ LEDs may become a critical issue, depending on LED dimension and separation, duration of optical stimulation, and material selection.

It is important to note that the majority of the devices surveyed in this paper are still at the early stage of development and mostly evaluated as successful in short-term animal studies that last only several days or weeks. A series of scientific and technical challenges need to be considered before such devices can be used for chronic experiments in freely moving animals. The most important practical consideration perhaps is the reliability and biocompatibility of the implanted devices, which can benefit from advances in biomaterials and packaging techniques. In addition, optogenetically induced behavior has been found to be relatively difficult in non-human primates, which may be related to sparse

volumetric photon stimulation of brain tissue.<sup>35,37,129</sup> This will present a significant challenge to using miniaturized optical devices in behavioral studies. Possible strategies for achieving a greater volumetric recruitment of excitable tissue may include increasing the density and scale of microdevices, designing new device structures to improve optical throughput and coverage, and revising experimental paradigms for device placement and operation. In short, engineering the development of highly efficient light delivery devices with increasing spatial resolution and scalability is likely to continue as an on-going research endeavor for the near future. Multifunctional components, such as microfluidics, thermal sensors, and strain sensors, may be combined with optical and electrical components to achieve complex system functionality. This will open up a new line of engineering research in the development of materials, models of optics, microfabrication methods, low-power RF microelectronic circuits, integration and packaging technologies, and surgical tools.

Besides the engineering development of microdevices, considerably more work on neuroscience is necessary for further transferring optogenetics tools to human trials. Optogenetics requires genetic intervention by light-sensitive DNA segments, which results in irreversible and permanent modification of the human nervous system.<sup>130</sup> The long-term safety evaluation of injected viral vectors and transfected light-gated ion channels are ethical and scientifically necessary.<sup>131</sup> So far, the safety of a non-optogenetic adeno-associated virus (AAV) has been tested in the retina of human participants, where no side effects have been reported and restoration of vision function has been observed in several trials.<sup>132–135</sup> The effort to design a first-in-human optogenetics trial has already begun.<sup>130</sup> There are other considerations of efficiency and long-term efficacy of optogenetic gene expression in humans. While still in its infancy, highly efficient opsins have been engineered and investigated to enable stable gene expression in non-human primates.<sup>136–138</sup> Further searching for new forms of energy-gated ion channels is potentially a new research trend. In summary, optogenetics has lighted a new pathway for dissecting neural circuitry in both healthy and diseased brains and enabled tremendous research opportunities in multidisciplinary areas of physics, engineering, materials science, and neuroscience.

## Acknowledgements

The authors acknowledge support from the National Science Foundation under the Award Numbers CBET-1264772 and ECCS-1407880.

## Notes and references

- 1 Z. Fekete, *Sens. Actuators, B*, 2015, **215**, 300–315.
- 2 S. F. Cogan, *Annu. Rev. Biomed. Eng.*, 2008, **10**, 275–309.
- 3 S. Butovas and C. Schwarz, *J. Neurophysiol.*, 2003, **90**, 3024–3039.

- 4 R. L. Fork, *Science*, 1971, **171**, 907–908.
- 5 G. Nagel, T. Szellas, W. Huhn, S. Kateriya, N. Adeishvili, P. Berthold, D. Ollig, P. Hegemann and E. Bamberg, *Proc. Natl. Acad. Sci. U. S. A.*, 2003, **100**, 13940–13945.
- 6 B. Schobert and J. K. Lanyi, *J. Biol. Chem.*, 1982, **257**, 10306–10313.
- 7 B. Y. Chow, X. Han, A. S. Dobry, X. Qian, A. S. Chuong, M. Li, M. A. Henninger, G. M. Belfort, Y. Lin, P. E. Monahan and E. S. Boyden, *Nature*, 2010, **463**, 98–102.
- 8 E. S. Boyden, F. Zhang, E. Bamberg, G. Nagel and K. Deisseroth, *Nat. Neurosci.*, 2005, **8**, 1263–1268.
- 9 F. Zhang, L.-P. Wang, M. Brauner, J. F. Liewald, K. Kay, N. Watzke, P. G. Wood, E. Bamberg, G. Nagel, A. Gottschalk and K. Deisseroth, *Nature*, 2007, **446**, 633–639.
- 10 V. Gradinaru, F. Zhang, C. Ramakrishnan, J. Mattis, R. Prakash, I. Diester, I. Goshen, K. R. Thompson and K. Deisseroth, *Cell*, 2010, **141**, 154–165.
- 11 F. Zhang, V. Gradinaru, A. R. Adamantidis, R. Durand, R. D. Airan, L. de Lecea and K. Deisseroth, *Nat. Protoc.*, 2010, **5**, 439–456.
- 12 V. Gradinaru, K. R. Thompson, F. Zhang, M. Mogri, K. Kay, M. B. Schneider and K. Deisseroth, *J. Neurosci.*, 2007, **27**, 14231–14238.
- 13 L. Fenno, O. Yizhar and K. Deisseroth, *Annu. Rev. Neurosci.*, 2011, **34**, 389–412.
- 14 M. R. Warden, J. A. Cardin and K. Deisseroth, *Annu. Rev. Biomed. Eng.*, 2014, **16**, 103–129.
- 15 J. M. Barrett, R. Berlinguer-Palmini and P. Degenaar, *Vis. Neurosci.*, 2014, **31**, 345–354.
- 16 P. R. Albert, *J. Psychiatry Neurosci.*, 2014, **39**, 3–5.
- 17 J. T. Paz and J. R. Huguenard, *Epilepsy Curr.*, 2015, **15**, 34–38.
- 18 C. M. Ambrosi, A. Klimas, J. Yu and E. Entcheva, *Prog. Biophys. Mol. Biol.*, 2014, **115**, 294–304.
- 19 F. Zhang, V. Gradinaru, A. R. Adamantidis, R. Durand, R. D. Airan, L. de Lecea and K. Deisseroth, *Nat. Protoc.*, 2010, **5**, 439–456.
- 20 O. Yizhar, L. E. Fenno, T. J. Davidson, M. Mogri and K. Deisseroth, *Neuron*, 2011, **71**, 9–34.
- 21 F. Zhang, A. M. Aravanis, A. Adamantidis, L. de Lecea and K. Deisseroth, *Nat. Rev. Neurosci.*, 2007, **8**, 577–581.
- 22 A. Dawydow, R. Gueta, D. Ljaschenko, S. Ullrich, M. Hermann, N. Ehmann, S. Gao, A. Fiala, T. Langenhan, G. Nagel and R. J. Kittel, *Proc. Natl. Acad. Sci. U. S. A.*, 2014, **111**, 13972–13977.
- 23 J. Y. Lin, P. M. Knutson, A. Muller, D. Kleinfeld and R. Y. Tsien, *Nat. Neurosci.*, 2013, **16**, 1499–1508.
- 24 A. S. Chuong, M. L. Miri, V. Busskamp, G. A. C. Matthews, L. C. Acker, A. T. Sørensen, A. Young, N. C. Klapoetke, M. A. Henninger, S. B. Kodandaramaiah, M. Ogawa, S. B. Ramanlal, R. C. Bandler, B. D. Allen, C. R. Forest, B. Y. Chow, X. Han, Y. Lin, K. M. Tye, B. Roska, J. A. Cardin and E. S. Boyden, *Nat. Neurosci.*, 2014, **17**, 1123–1129.
- 25 T. Ishizuka, M. Kakuda, R. Araki and H. Yawo, *Neurosci. Res.*, 2006, **54**, 85–94.
- 26 B. E. Losavio, V. Iyer, S. Patel and P. Saggau, *J. Neural Eng.*, 2010, **7**, 045002.
- 27 A. B. Arrenberg, D. Y. R. Stainier, H. Baier and J. Huisken, *Science*, 2010, **330**, 971–974.
- 28 P. Zhu, O. Fajardo, J. Shum, Y.-P. Zhang Schärer and R. W. Friedrich, *Nat. Protoc.*, 2012, **7**, 1410–1425.
- 29 A. M. Aravanis, L.-P. Wang, F. Zhang, L. A. Meltzer, M. Z. Mogri, M. B. Schneider and K. Deisseroth, *J. Neural Eng.*, 2007, **4**, S143–S156.
- 30 R. D. Airan, K. R. Thompson, L. E. Fenno, H. Bernstein and K. Deisseroth, *Nature*, 2009, **458**, 1025–1029.
- 31 P. Anikeeva, A. S. Andelman, I. Witten, M. Warden, I. Goshen, L. Grosenick, L. A. Gunaydin, L. M. Frank and K. Deisseroth, *Nat. Neurosci.*, 2012, **15**, 163–170.
- 32 J. A. Cardin, M. Carlén, K. Meletis, U. Knoblich, F. Zhang, K. Deisseroth, L.-H. Tsai and C. I. Moore, *Nat. Protoc.*, 2010, **5**, 247–254.
- 33 D. F. English, O. Ibanez-Sandoval, E. Stark, F. Tecuapetla, G. Buzsáki, K. Deisseroth, J. M. Tepper and T. Koos, *Nat. Neurosci.*, 2012, **15**, 123–130.
- 34 K. R. Dhakal, L. Gu, S. Shivalingaiah, T. S. Dennis, S. A. Morris-Bobzean, T. Li, L. I. Perrotti and S. K. Mohanty, *PLoS One*, 2014, **9**, e111488.
- 35 X. Han, X. Qian, J. G. Bernstein, H.-H. Zhou, G. T. Franzesi, P. Stern, R. T. Bronson, A. M. Graybiel, R. Desimone and E. S. Boyden, *Neuron*, 2009, **62**, 191–198.
- 36 I. Ozden, J. Wang, Y. Lu, T. May, J. Lee, W. Goo, D. J. O'Shea, P. Kalanithi, I. Diester, M. Diagne, K. Deisseroth, K. V. Shenoy and A. V. Nurmikko, *J. Neurosci. Methods*, 2013, **219**, 142–154.
- 37 I. Diester, M. T. Kaufman, M. Mogri, R. Pashaie, W. Goo, O. Yizhar, C. Ramakrishnan, K. Deisseroth and K. V. Shenoy, *Nat. Neurosci.*, 2011, **14**, 387–397.
- 38 O. Ruiz, B. R. Lustig, J. J. Nassi, A. Cetin, J. H. Reynolds, T. D. Albright, E. M. Callaway, G. R. Stoner and A. W. Roe, *J. Neurophysiol.*, 2013, **110**, 1455–1467.
- 39 E. Stark, T. Koos and G. Buzsáki, *J. Neurophysiol.*, 2012, **108**, 349–363.
- 40 A. M. Aravanis, L.-P. Wang, F. Zhang, L. A. Meltzer, M. Z. Mogri, M. B. Schneider and K. Deisseroth, *J. Neural Eng.*, 2007, **4**, S143–S156.
- 41 Y. LeChasseur, S. Dufour, G. Lavertu, C. Bories, M. Deschênes, R. Vallée and Y. De Koninck, *Nat. Methods*, 2011, **8**, 319–325.
- 42 S. Dufour, G. Lavertu, S. Dufour-Beausejour, A. Juneau-Fecteau, N. Calakos, M. Deschênes, R. Vallée and Y. De Koninck, *PLoS One*, 2013, **8**, e57703.
- 43 K. Tamura, Y. Ohashi, T. Tsubota, D. Takeuchi, T. Hirabayashi, M. Yaguchi, M. Matsuyama, T. Sekine and Y. Miyashita, *J. Neurosci. Methods*, 2012, **211**, 49–57.
- 44 T. V. F. Abaya, M. Diwekar, S. Blair, P. Tathireddy, L. Rieth, G. A. Clark and F. Solzbacher, *Biomed. Opt. Express*, 2012, **3**, 2200–2219.
- 45 T. V. F. Abaya, S. Blair, P. Tathireddy, L. Rieth and F. Solzbacher, *Biomed. Opt. Express*, 2012, **3**, 3087–3104.

- 46 J. Zhang, F. Laiwalla, J. A. Kim, H. Urabe, R. Van Wagenen, Y.-K. Song, B. W. Connors, F. Zhang, K. Deisseroth and A. V. Nurmikko, *J. Neural Eng.*, 2009, **6**, 055007.
- 47 J. Zhang, F. Laiwalla, J. A. Kim, H. Urabe, R. Van Wagenen, Y.-K. Song, B. W. Connors and A. V. Nurmikko, *Conf. Proc. IEEE Eng. Med. Biol. Soc.*, 2009, **2009**, 2046–2049.
- 48 J. Wang, I. Ozden, M. Diagne, F. Wagner, D. Borton, B. Brush, N. Agha, R. Burwell, D. Sheinberg, I. Diester, K. Deisseroth and A. Nurmikko, *Conf. Proc. IEEE Eng. Med. Biol. Soc.*, 2011, **2011**, 7525–7528.
- 49 J. Wang, F. Wagner, D. A. Borton, J. Zhang, I. Ozden, R. D. Burwell, A. V. Nurmikko, R. van Wagenen, I. Diester and K. Deisseroth, *J. Neural Eng.*, 2012, **9**, 016001.
- 50 F. Wu, E. Stark, M. Im, I.-J. Cho, E.-S. Yoon, G. Buzsáki, K. D. Wise and E. Yoon, *J. Neural Eng.*, 2013, **10**, 056012.
- 51 M. Schwaerzle, K. Seidl, U. T. Schwarz, O. Paul and P. Ruther, in *2013 IEEE 26th International Conference on Micro Electro Mechanical Systems (MEMS)*, 2013, pp. 1029–1032.
- 52 B. Rubehn, S. B. E. Wolff, P. Toyote, M. Schuettler, A. Lüthi and T. Stieglitz, *Conf. Proc. IEEE Eng. Med. Biol. Soc.*, 2011, **2011**, 2969–2972.
- 53 Y. Son, H. J. Lee, J. Kim, C. J. Lee, E.-S. Yoon, T. G. Kim and I.-J. Cho, in *2015 28th IEEE International Conference on Micro Electro Mechanical Systems (MEMS)*, 2015, pp. 158–161.
- 54 K. D. Wise, J. B. Angell and A. Starr, *IEEE Trans. Biomed. Eng.*, 1970, **BME-17**, 238–247.
- 55 A. N. Zorzos, E. S. Boyden and C. G. Fonstad, *Opt. Lett.*, 2010, **35**, 4133–4135.
- 56 C.-W. Chang and J.-C. Chiou, *Sensors*, 2010, **10**, 4238–4252.
- 57 J. John, Y. Li, J. Zhang, J. A. Loeb and Y. Xu, *J. Micromech. Microeng.*, 2011, **21**, 105011.
- 58 Y. Yao, M. N. Gulari, J. A. Wiler and K. D. Wise, *J. Microelectromech. Syst.*, 2007, **16**, 977–988.
- 59 A. N. Zorzos, J. Scholvin, E. S. Boyden and C. G. Fonstad, *Opt. Lett.*, 2012, **37**, 4841–4843.
- 60 F. Pisanello, L. Sileo, I. A. Oldenburg, M. Pisanello, L. Martiradonna, J. A. Assad, B. L. Sabatini and M. De Vittorio, *Neuron*, 2014, **82**, 1245–1254.
- 61 Y. Iwai, S. Honda, H. Ozeki, M. Hashimoto and H. Hirase, *Neurosci. Res.*, 2011, **70**, 124–127.
- 62 S. K. Mohanty and N. V. Thakor, *Proc. SPIE*, 2013, **8586**, 1–10.
- 63 J. G. McCall, T. Kim, G. Shin, X. Huang, Y. H. Jung, R. Al-Hasani, F. G. Omenetto, M. R. Bruchas and J. A. Rogers, *Nat. Protoc.*, 2013, **8**, 2413–2428.
- 64 L. Campagnola, H. Wang and M. J. Zylka, *J. Neurosci. Methods*, 2008, **169**, 27–33.
- 65 T. Ishizuka, M. Kakuda, R. Araki and H. Yawo, *Neurosci. Res.*, 2006, **54**, 85–94.
- 66 C.-W. Jeon, K.-S. Kim and M. D. Dawson, *Phys. Status Solidi A*, 2002, **192**, 325–328.
- 67 H. X. Zhang, D. Massoubre, J. McKendry, Z. Gong, B. Guilhabert, C. Griffin, E. Gu, P. E. Jessop, J. M. Girkin and M. D. Dawson, *Opt. Express*, 2008, **16**, 9918–9926.
- 68 T. Kim, Y. H. Jung, J. Song, D. Kim, Y. Li, H. Kim, I.-S. Song, J. J. Wierer, H. A. Pao, Y. Huang and J. A. Rogers, *Small*, 2012, **8**, 1643–1649.
- 69 K. E. Jones, P. K. Campbell and R. A. Normann, *Ann. Biomed. Eng.*, 1992, **20**, 423–437.
- 70 A. Branner, R. B. Stein and R. A. Normann, *J. Neurophysiol.*, 2001, **85**, 1585–1594.
- 71 A. Branner and R. A. Normann, *Brain Res. Bull.*, 2000, **51**, 293–306.
- 72 P. Degenaar, B. McGovern, R. Berlinguer-Palmini, N. Vysokov, N. Grossman, V. Pohrer, E. Drakakis and M. Neil, in *2010 IEEE Biomedical Circuits and Systems Conference (BioCAS)*, 2010, pp. 170–173.
- 73 N. Grossman, V. Poher, M. S. Grubb, G. T. Kennedy, K. Nikolic, B. McGovern, R. B. Palmini, Z. Gong, E. M. Drakakis, M. A. A. Neil, M. D. Dawson, J. Burrone and P. Degenaar, *J. Neural Eng.*, 2010, **7**, 016004.
- 74 H. W. Choi, C. W. Jeon and M. D. Dawson, *J. Cryst. Growth*, 2004, **268**, 527–530.
- 75 O. Yizhar, L. E. Fenno, T. J. Davidson, M. Mogri and K. Deisseroth, *Neuron*, 2011, **71**, 9–34.
- 76 C. Hassler, T. Boretius and T. Stieglitz, *J. Polym. Sci., Part B: Polym. Phys.*, 2011, **49**, 18–33.
- 77 K. Y. Kwon, B. Sirowatka, W. Li and A. Weber, *2012 IEEE Biomed. Circuits Syst Conf BioCAS*, 2012, pp. 164–167.
- 78 K. Y. Kwon, B. Sirowatka, A. Weber and W. Li, *IEEE Trans. Biomed. Circuits Syst.*, 2013, **7**, 593–600.
- 79 M. Schwaerzle, P. Elmlinger, O. Paul and P. Ruther, in *2014 36th Annual International Conference of the IEEE Engineering in Medicine and Biology Society (EMBC)*, 2014, pp. 5252–5255.
- 80 M. Schwaerzle, P. Elmlinger, O. Paul and P. Ruther, in *2015 28th IEEE International Conference on Micro Electro Mechanical Systems (MEMS)*, 2015, pp. 162–165.
- 81 K. Y. Kwon, H.-M. Lee, M. Ghovanloo, A. Weber and W. Li, *Front. Syst. Neurosci.*, 2015, **69**.
- 82 K. Y. Kwon, A. Weber and W. Li, *J. Microelectromech. Syst.*, 2014, **23**, 1272–1280.
- 83 H.-M. Lee, K. Y. Kwon, W. Li and M. Ghovanloo, *IEEE J. Solid-State Circuits*, 2015, **50**, 360–374.
- 84 K. Kwon and W. Li, in *2013 IEEE 26th International Conference on Micro Electro Mechanical Systems (MEMS)*, 2013, pp. 1017–1020.
- 85 K. Y. Kwon, A. Khomenko, M. Haq and W. Li, in *2013 35th Annual International Conference of the IEEE Engineering in Medicine and Biology Society (EMBC)*, 2013, pp. 249–252.
- 86 K. Y. Kwon, H.-M. Lee, M. Ghovanloo, A. Weber and W. Li, in *2014 IEEE 27th International Conference on Micro Electro Mechanical Systems (MEMS)*, 2014, pp. 813–816.
- 87 K. Y. Kwon, X. Bi and W. Li, in *2013 35th Annual International Conference of the IEEE Engineering in Medicine and Biology Society (EMBC)*, 2013, pp. 767–770.
- 88 G. Keiser, *Optical Fiber Comm*, McGraw-Hill, New York, 4th edn, 2008.
- 89 H. Cao, L. Gu, S. K. Mohanty and J.-C. Chiao, *IEEE Trans. Biomed. Eng.*, 2013, **60**, 225–229.
- 90 B. Fan, K. Y. Kwon, A. J. Weber and W. Li, in *2014 36th Annual International Conference of the IEEE Engineering in Medicine and Biology Society (EMBC)*, 2014, pp. 450–453.

- 91 N. McAlinden, D. Massoubre, E. Richardson, E. Gu, S. Sakata, M. D. Dawson and K. Mathieson, *Opt. Lett.*, 2013, **38**, 992–994.
- 92 N. McAlinden, E. Gu, M. D. Dawson, S. Sakata and K. Mathieson, *Front. Neural Circuits*, 2015, **9**, 00025.
- 93 T. Kim, J. G. McCall, Y. H. Jung, X. Huang, E. R. Siuda, Y. Li, J. Song, Y. M. Song, H. A. Pao, R.-H. Kim, C. Lu, S. D. Lee, I.-S. Song, G. Shin, R. Al-Hasani, S. Kim, M. P. Tan, Y. Huang, F. G. Omenetto, J. A. Rogers and M. R. Bruchas, *Science*, 2013, **340**, 211–216.
- 94 M. A. Rossi, V. Go, T. Murphy, Q. Fu, J. Morizio and H. H. Yin, *Front. Integr. Neurosci.*, 2015, **9**, 8.
- 95 M. Hashimoto, A. Hata, T. Miyata and H. Hirase, *Neurophotonics*, 2014, **1**, 011002–011002.
- 96 S. T. Lee, P. A. Williams, C. E. Braine, D.-T. Lin, S. W. M. John and P. P. Irazoqui, *IEEE Trans. Neural Syst. Rehabil. Eng.*, 2015, **1**.
- 97 C. T. Wentz, J. G. Bernstein, P. Monahan, A. Guerra, A. Rodriguez and E. S. Boyden, *J. Neural Eng.*, 2011, **8**, 046021.
- 98 R. Ameli, A. Mirbozorgi, J.-L. Neron, Y. Lechasseur and B. Gosselin, *Conf. Proc. IEEE Eng. Med. Biol. Soc.*, 2013, **2013**, 5662–5665.
- 99 P. Andersen and E. I. Moser, *Hippocampus*, 1995, **5**, 491–498.
- 100 C. Childs, *Br. J. Neurosurg.*, 2008, **22**, 486–496.
- 101 Y. Li, X. Shi, J. Song, C. Lü, T. Kim, J. G. McCall, M. R. Bruchas, J. A. Rogers and Y. Huang, *Proc. R. Soc. London, Ser. A*, 2013, **469**, 20130142.
- 102 Y. Li, Y. Shi, J. Song, C. Lu, T. Kim, J. A. Rogers and Y. Huang, *J. Appl. Phys.*, 2013, **113**, 144505.
- 103 B. Fan, K.-Y. Kwon, R. Rechenberg, A. Khomenko, M. Haq, M. F. Becker, A. J. Weber and W. Li, in *2015 28th IEEE International Conference on Micro Electro Mechanical Systems (MEMS)*, 2015, pp. 616–619.
- 104 S. V. Kidalov and F. M. Shakhov, *Materials*, 2009, **2**, 2467–2495.
- 105 M. Hupert, A. Muck, J. Wang, J. Stotter, Z. Cvackova, S. Haymond, Y. Show and G. M. Swain, *Diamond Relat. Mater.*, 2003, **12**, 1940–1949.
- 106 A. Kraft, *Int. J. Electrochem. Sci.*, 2007, **2**, 355–385.
- 107 Open Optogenetics—the optogenetics wiki.,
- 108 A. Galvan, X. Hu, Y. Smith and T. Wichmann, *PLoS One*, 2012, **7**, e50808.
- 109 X. Han, *ACS Chem. Neurosci.*, 2012, **3**, 577–584.
- 110 K. Honda, *J. Photochem. Photobiol.*, 2004, **166**, 63–68.
- 111 A. N. Zorzos, A. Dietrich, G. Talei Franzesi, B. Y. Chow, X. Han, C. G. Fonstad and E. S. Boyden, *Soc. Neurosci.*, 2009, **388**, GG107.
- 112 D.-W. Park, A. A. Schendel, S. Mikael, S. K. Brodnick, T. J. Richner, J. P. Ness, M. R. Hayat, F. Atry, S. T. Frye, R. Pashaie, S. Thongpang, Z. Ma and J. C. Williams, *Nat. Commun.*, 2014, **5**, 5258.
- 113 E. Fiedler, N. Haas and T. Stieglitz, *Conf. Proc. IEEE Eng. Med. Biol. Soc.*, 2014, **2014**, 438–441.
- 114 L. Eldada and L. W. Shacklette, *IEEE J. Sel. Top. Quantum Electron.*, 2000, **6**, 54–68.
- 115 M. Vogt and R. Hauptmann, *Surf. Coat. Technol.*, 1995, **74**–75(Part 2), 676–681.
- 116 J. Subbaroyan, D. C. Martin and D. R. Kipke, *J. Neural Eng.*, 2005, **2**, 103–113.
- 117 V. S. Polikov, P. A. Tresco and W. M. Reichert, *J. Neurosci. Methods*, 2005, **148**, 1–18.
- 118 J. P. Harris, J. R. Capadona, R. H. Miller, B. C. Healy, K. Shanmuganathan, S. J. Rowan, C. Weder and D. J. Tyler, *J. Neural Eng.*, 2011, **8**, 066011.
- 119 D.-H. Kim, J. Viventi, J. J. Amsden, J. Xiao, L. Vigeland, Y.-S. Kim, J. A. Blanco, B. Panilaitis, E. S. Frechette, D. Contreras, D. L. Kaplan, F. G. Omenetto, Y. Huang, K.-C. Hwang, M. R. Zakin, B. Litt and J. A. Rogers, *Nat. Mater.*, 2010, **9**, 511–517.
- 120 F. Barz, P. Ruther, S. Takeuchi and O. Paul, in *2015 28th IEEE International Conference on Micro Electro Mechanical Systems (MEMS)*, 2015, pp. 636–639.
- 121 Dow.com <http://www.dow.com/polyglycols/polyethylene/products/carbowaxp.htm>.
- 122 G. Jiang and D. D. Zhou, in *Implantable Neural Prostheses 2*, ed. D. Zhou and E. Greenbaum, Springer, New York, 2009, pp. 27–61.
- 123 T. Stieglitz, Methods to determine the stability of polymer encapsulations, *The 10th annual conference of the international functional electrical stimulation society*, Montréal, Canada, 2005.
- 124 M. Kazemi, E. Basham, M. Sivaprakasam, G. Wang, D. Rodger, J. Weiland, Y. C. Tai, W. Liu and M. Humayun, in *26th Annual International Conference of the IEEE Engineering in Medicine and Biology Society, 2004. IEMBS '04*, 2004, vol. 2, pp. 4093–4095.
- 125 X. Xie, L. Rieth, L. Williams, S. Negi, R. Bhandari, R. Caldwell, R. Sharma, P. Tathireddy and F. Solzbacher, *J. Neural Eng.*, 2014, **11**, 026016.
- 126 Y. Xie, N. Martini, C. Hassler, R. D. Kirch, T. Stieglitz, A. Seifert and U. G. Hofmann, *Front. Neuroeng.*, 2014, **7**, 00034.
- 127 P. Fattah, G. Yang, G. Kim and M. R. Abidian, *Adv. Mater.*, 2014, **26**, 1846–1885.
- 128 J. M. Morais, F. Papadimitrakopoulos and D. J. Burgess, *AAPS J.*, 2010, **12**, 188–196.
- 129 A. Gerits, R. Farivar, B. R. Rosen, L. L. Wald, E. S. Boyden and W. Vanduffel, *Curr. Biol.*, 2012, **22**, 1722–1726.
- 130 F. Gilbert, A. R. Harris and R. M. I. Kapsa, *AJOB Neurosci.*, 2012, **3**, 20–22.
- 131 F. Bretzner, F. Gilbert, F. Baylis and R. M. Brownstone, *Cell Stem Cell*, 2011, **8**, 468–475.
- 132 F. Gilbert, A. R. Harris and R. M. I. Kapsa, *AJOB Neurosci.*, 2014, **5**, 3–11.
- 133 J. W. B. Bainbridge, A. J. Smith, S. S. Barker, S. Robbie, R. Henderson, K. Balaggan, A. Viswanathan, G. E. Holder, A. Stockman, N. Tyler, S. Petersen-Jones, S. S. Bhattacharya, A. J. Thrasher, F. W. Fitzke, B. J. Carter, G. S. Rubin, A. T. Moore and R. R. Ali, *N. Engl. J. Med.*, 2008, **358**, 2231–2239.
- 134 A. V. Cideciyan, W. W. Hauswirth, T. S. Aleman, S. Kaushal, S. B. Schwartz, S. L. Boye, E. A. M. Windsor, T. J. Conlon, A. Sumaroka, J.-J. Pang, A. J. Roman, B. J. Byrne and S. G. Jacobson, *Hum. Gene Ther.*, 2009, **20**, 999–1004.

- 135 F. Simonelli, A. M. Maguire, F. Testa, E. A. Pierce, F. Mingozi, J. L. Bennicelli, S. Rossi, K. Marshall, S. Banfi, E. M. Surace, J. Sun, T. M. Redmond, X. Zhu, K. S. Shindler, G.-S. Ying, C. Zivello, C. Acerra, J. F. Wright, J. W. McDonnell, K. A. High, J. Bennett and A. Auricchio, *Mol. Ther.*, 2010, **18**, 643–650.
- 136 X. Han, *Prog. Brain Res.*, 2012, **196**, 215–233.
- 137 A. Gerits and W. Vanduffel, *Trends Genet.*, 2013, **29**, 403–411.
- 138 R. Pashaie, P. Anikeeva, J. H. Lee, R. Prakash, O. Yizhar, M. Prigge, D. Chander, T. J. Richner and J. Williams, *IEEE Rev Biomed Eng*, 2014, **7**, 3–30.